Science Advances
AAAS

advances.sciencemag.org/cgi/content/full/7/12/eabf9153/DC1

Supplementary Materials for

Three-dimensional, multifunctional neural interfaces for cortical spheroids and engineered assembloids

Yoonseok Park, Colin K. Franz, Hanjun Ryu, Haiwen Luan, Kristen Y. Cotton, Jong Uk Kim, Ted S. Chung, Shiwei Zhao, Abraham Vazquez-Guardado, Da Som Yang, Kan Li, Raudel Avila, Jack K. Phillips, Maria J. Quezada, Hokyung Jang, Sung Soo Kwak, Sang Min Won, Kyeongha Kwon, Hyoyoung Jeong, Amay J. Bandodkar, Mengdi Han, Hangbo Zhao, Gabrielle R. Osher, Heling Wang, KunHyuck Lee, Yihui Zhang, Yonggang Huang*, John D. Finan*, John A. Rogers*

*Corresponding author. Email: y-huang@northwestern.edu (Y.H.); jdfinan@uic.edu (J.D.F.); jrogers@northwestern.edu (J.A.R.)

Published 17 March 2021, *Sci. Adv.* **7**, eabf9153 (2021)
DOI: 10.1126/sciadv.abf9153

The PDF file includes:

Other Supplementary Material for this manuscript includes the following:

(available at advances.sciencemag.org/cgi/content/full/7/12/eabf9153/DC1)

Movie S1. Transforming a microfabricated 2D structure into a 3D mesoscale multifunctional framework by compressive buckling.

Movie S2. Insertion of cortical spheroid into a 3D mesoscale multifunctional framework.

Movie S3. Representative firing and bursting events across the neural spheroid during 250 ms.

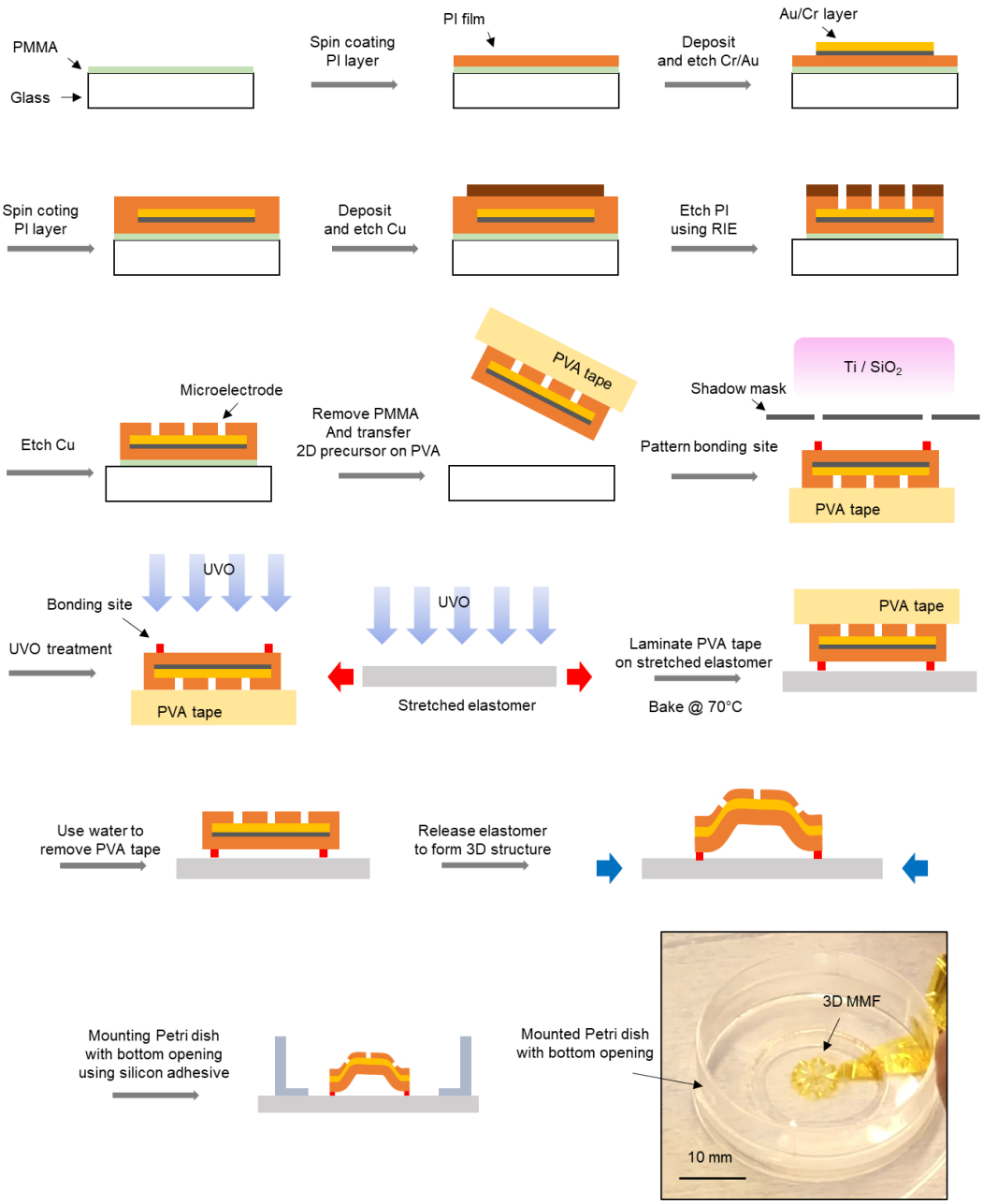

Fig. S1. **Procedure for fabricating 3D mesoscale multifunctional frameworks (3D MMFs) and optical image of a structure mounted on a petri-dish**. Schematic illustration of the steps for fabricating 3D MMFs and optical image of a 3D MMF mounted on a petri-dish with 2 mm bottom opening. Photo credit: Yoonseok Park, Northwestern University.

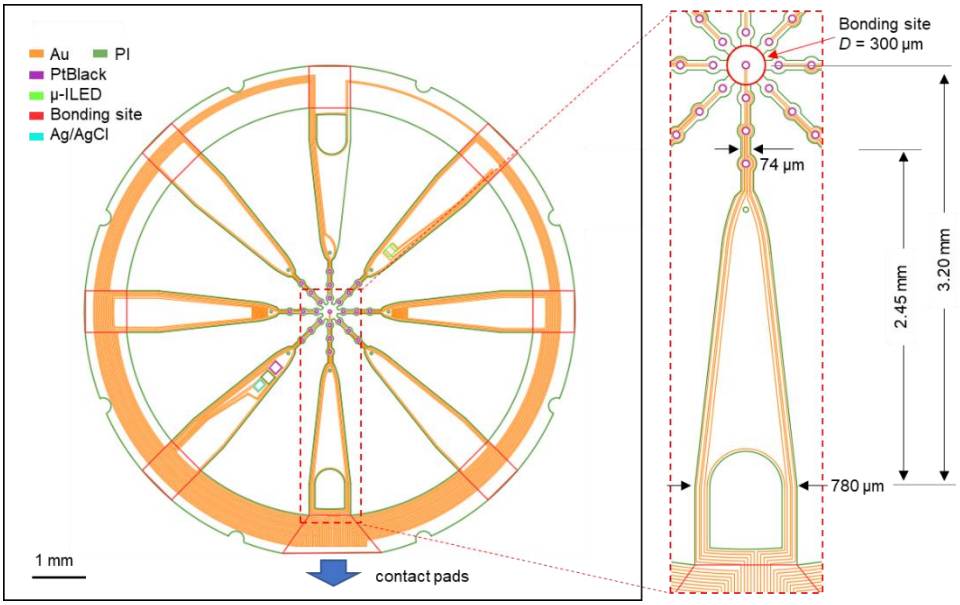

Fig. S2. The design of a 2D precursor for a single spheroid 3D MMF. Layouts of gold wires, polyimide, bonding sites and multifunctional devices.

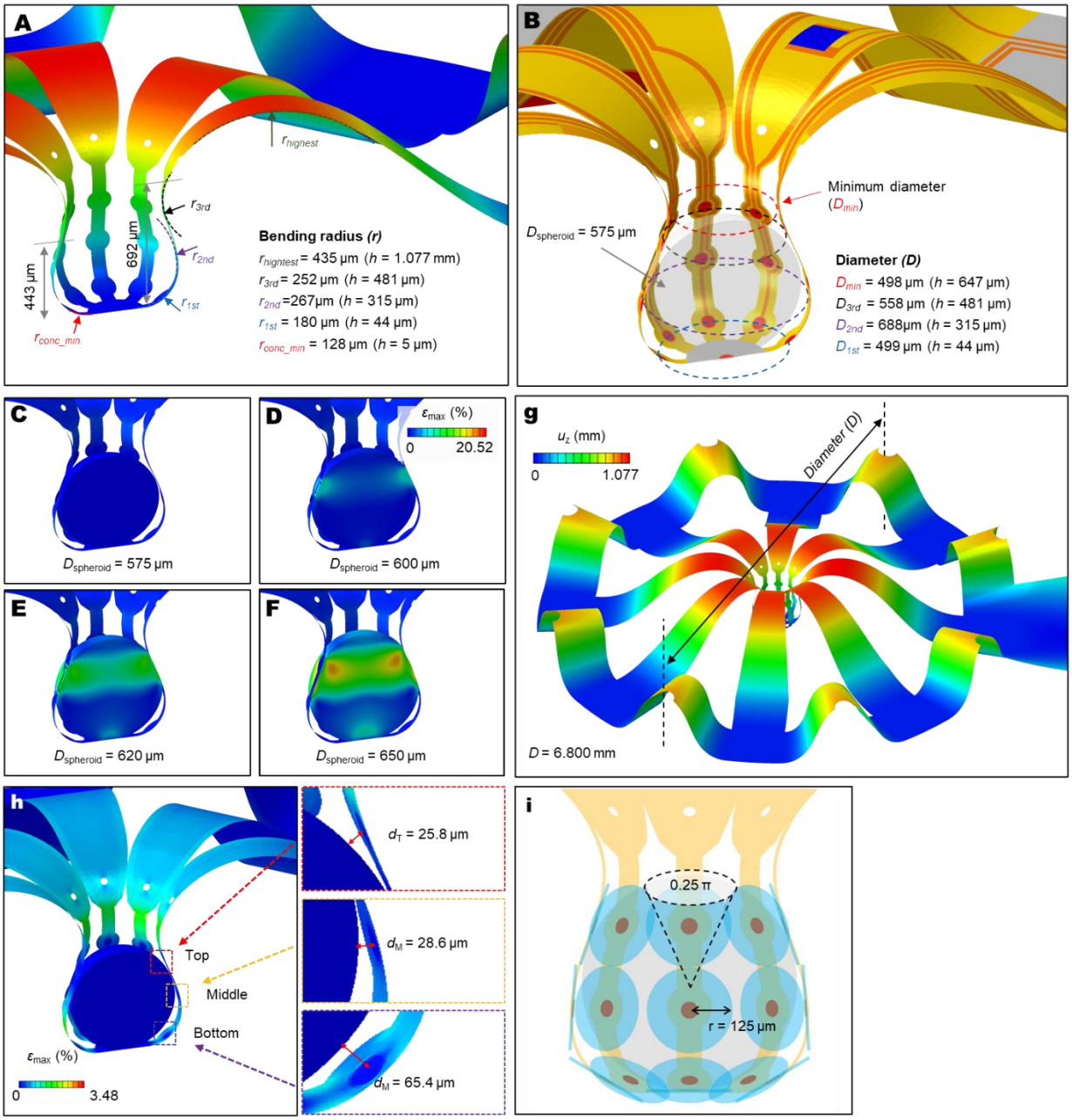

Fig. S3. **Key dimensional features of a 3D MMF predicted by FEA.** (**A**) Bending radii over the continuously curved 'wing' at each height. (**B**) The diameters of the enclosed space, at the heights of each set of electrodes. The maximum principal strain contours in the 3D MMF, after inserting cortical spheroids of (**C**) 575 µm (**D**) 600 µm (**E**) 620 µm (**F**) 650 µm in diameter. (**G**) Width and height of whole structure of 3D MMF. (**H**) Distances between the spheroid and the top, middle and bottom electrodes. (**I**) Solid angle of coverage across the spheroid with the assumption that each microelectrode can collect the field potential within a distance of 125 µm.

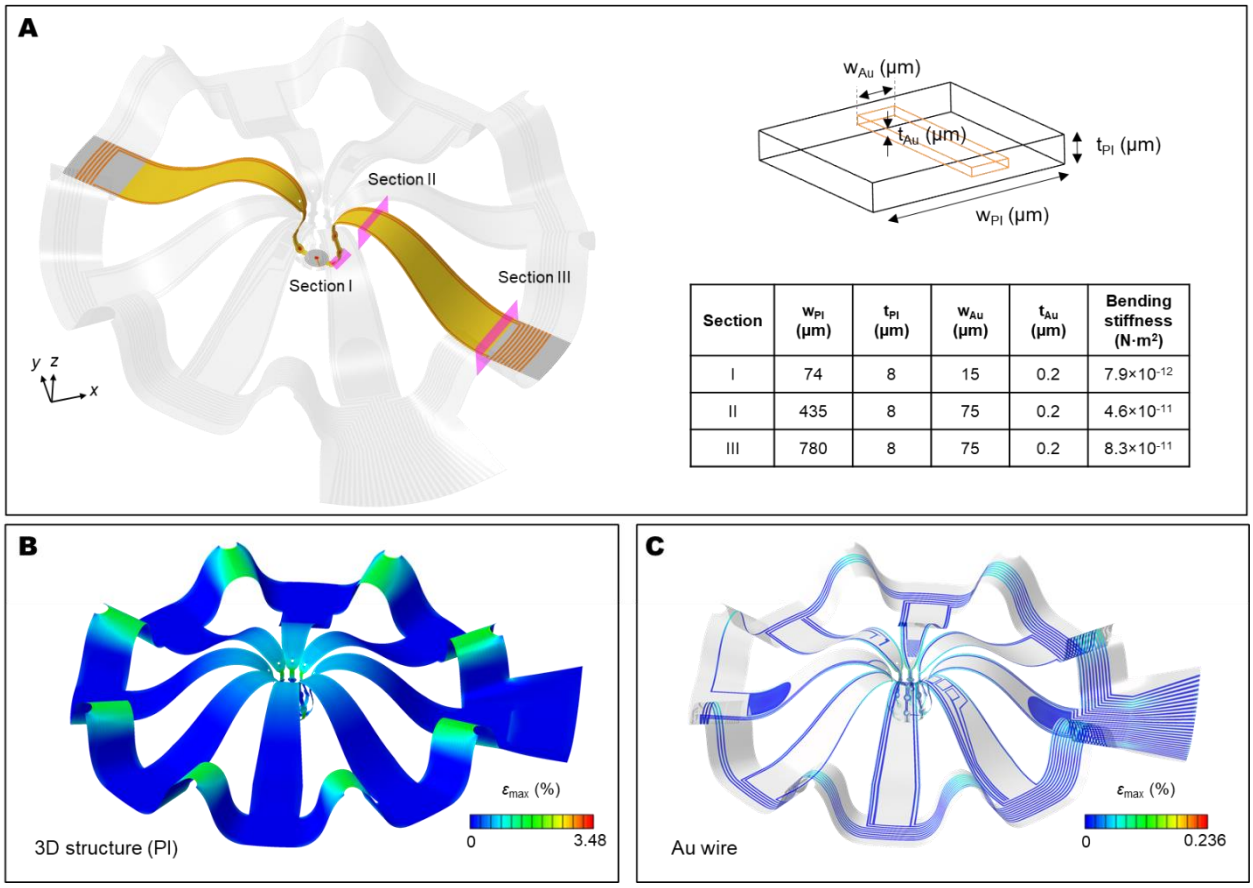

Section	w_{PI} (μm)	t_{PI} (μm)	w_{Au} (μm)	t_{Au} (μm)	Bending stiffness (N·m²)
I	74	8	15	0.2	7.9×10^{-12}
II	435	8	75	0.2	4.6×10^{-11}
III	780	8	75	0.2	8.3×10^{-11}

Fig. S4. **Mechanical behaviors of a 3D MMF predicted by FEA.** Maximum principal strain (A) across the entire 3D MMF and (**B**) along the gold wires embedded in PI. (**C**) Bending stiffnesses of the wings of the 3D MMF at three representative locations.

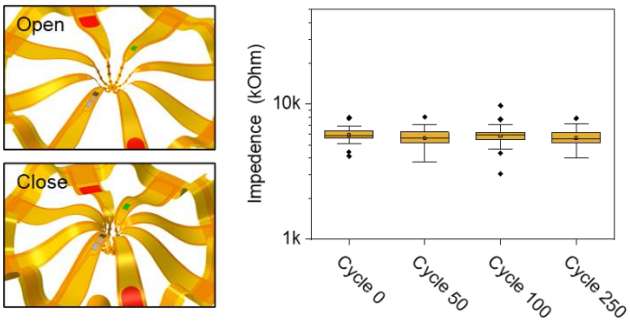

Fig. S5. Durability of the 3D MMF. Change in impedance over 250 cycles of opening and closing.

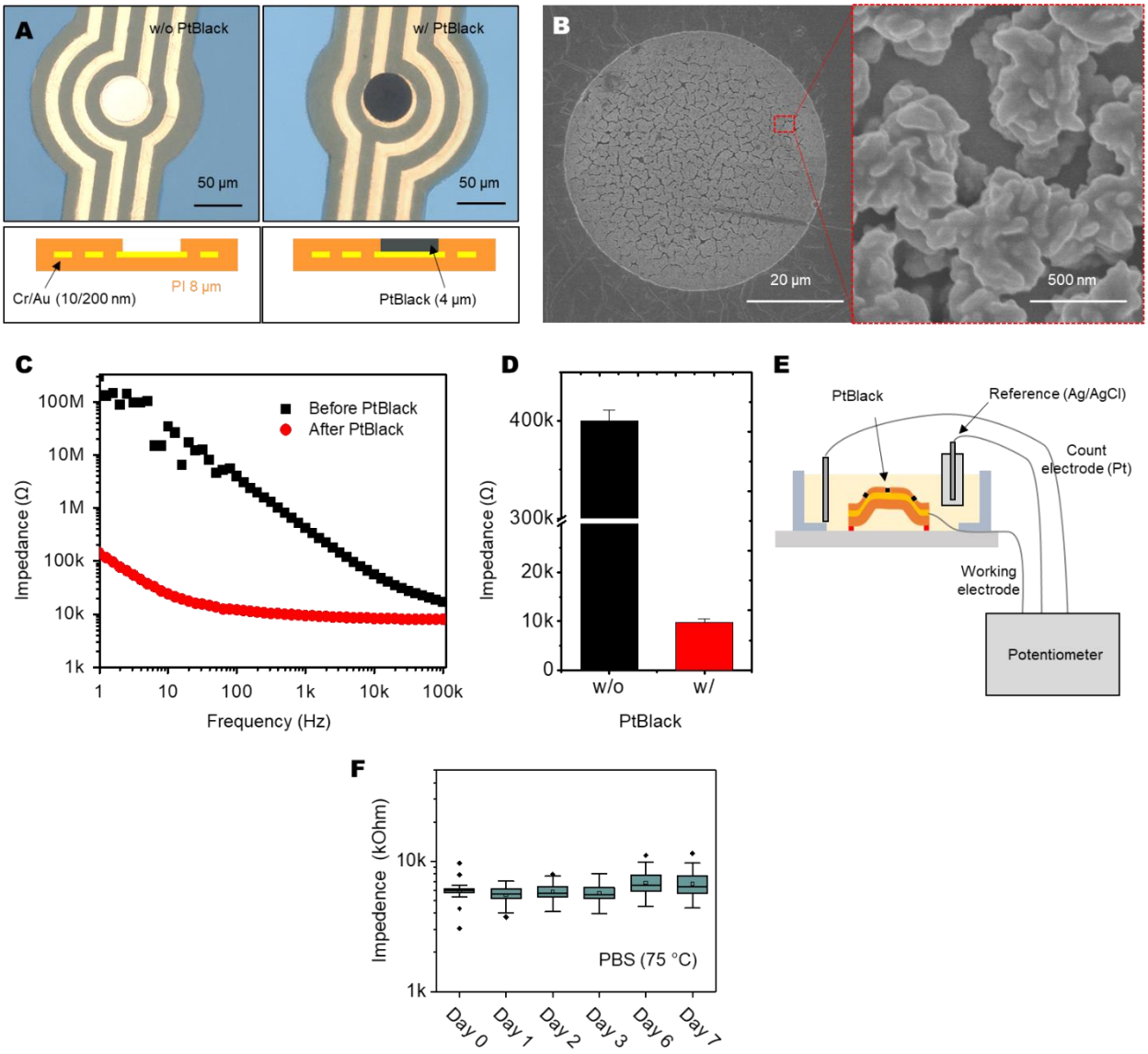

Fig. S6. **Electroplated microelectrodes for low impedance neural interfaces.** (**A**) Optical microscope image, schematic illustration and (**B**) SEM images of gold electrodes (50 μm in diameter; 200 nm in thickness) coated with porous platinum (PtBk; 50 μm in diameter; 4 μm in thickness). (**C**) Representative plot of impedance as a function of frequency before and after plating the layer of PtBk. (**D**) Averaged impedance of 25 electrodes before and after 20 s plating at 0.1V. (**E**) Schematic illustration of electroplating using a three-electrode system. (**F**) Change in impedance over 7 days after immersing into 75 °C PBS solution; 25 electrodes, mean ± s.d. Photo credit: Yoonseok Park, Northwestern University.

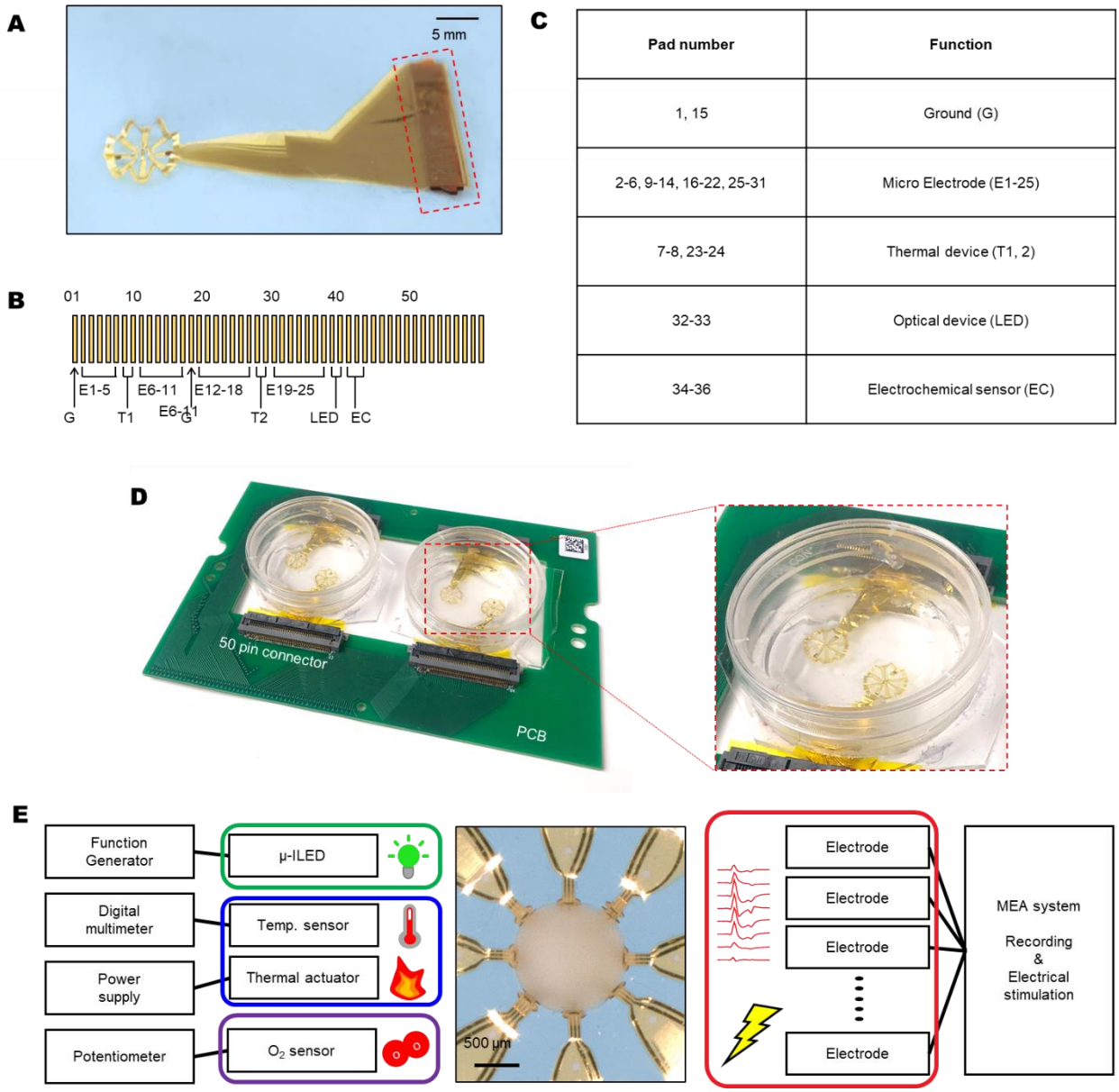

Fig. S7. **Optical images of key aspects of the system and its operation.** (**A**) Optical image of a 3D MMF with 50 contact pads and (**B**). Terminal sequence of the contact pads. (**C**) Addressing information for each contact pad. (**D**) Customized PCB with installation of four separate 3D MMF systems. (**E**) Block diagram showing optical, thermal, electrochemical and electrical functions integrated into a 3D MMF. Photo credit: Yoonseok Park, Northwestern University.

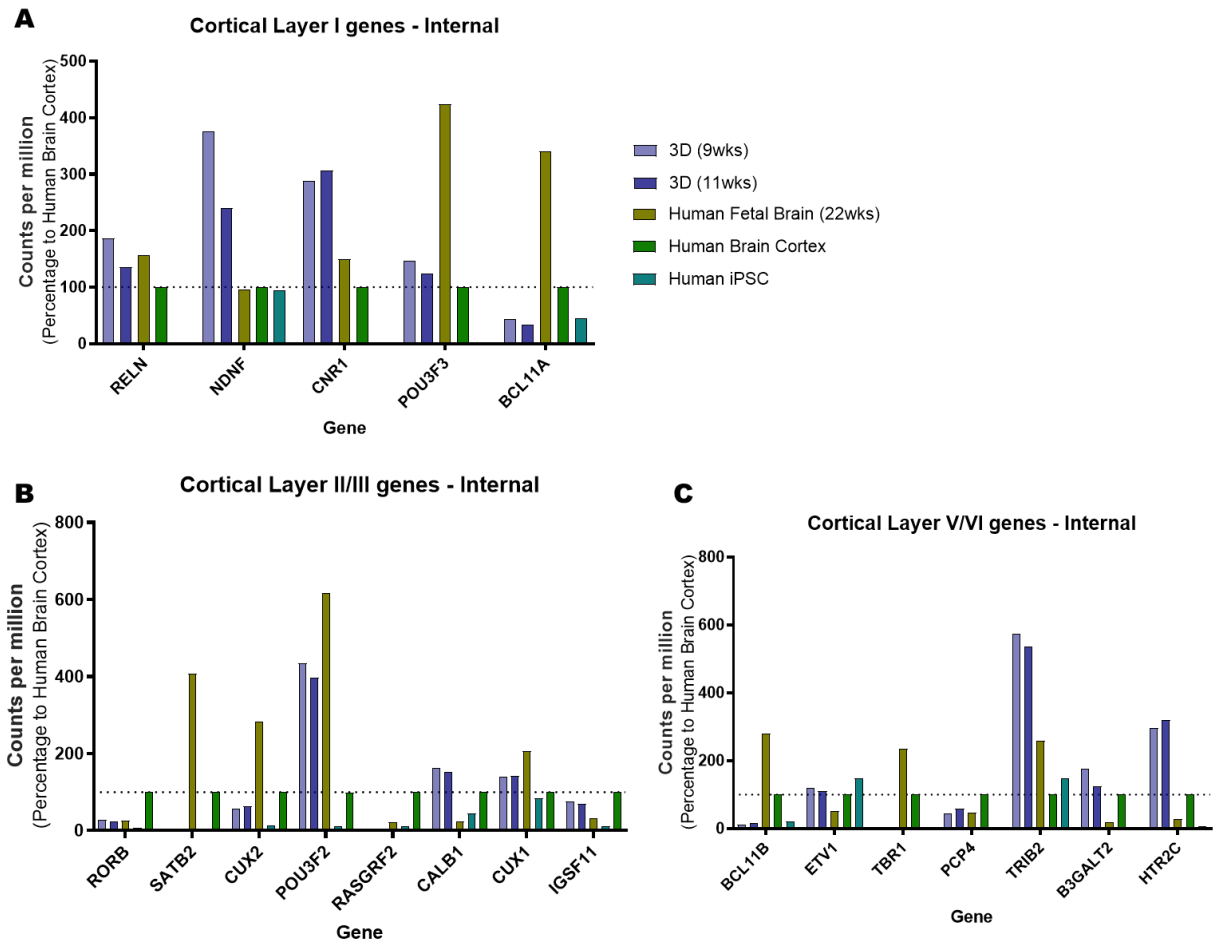

Fig. S8 RNA-Seq measurements of gene expression levels. RNA-Seq measurements of gene expression levels in spheroidal cultures for genes specific to (**A**) cortical layer I, (**B**) cortical layer II/III and (**C**) cortical layer V/VI.

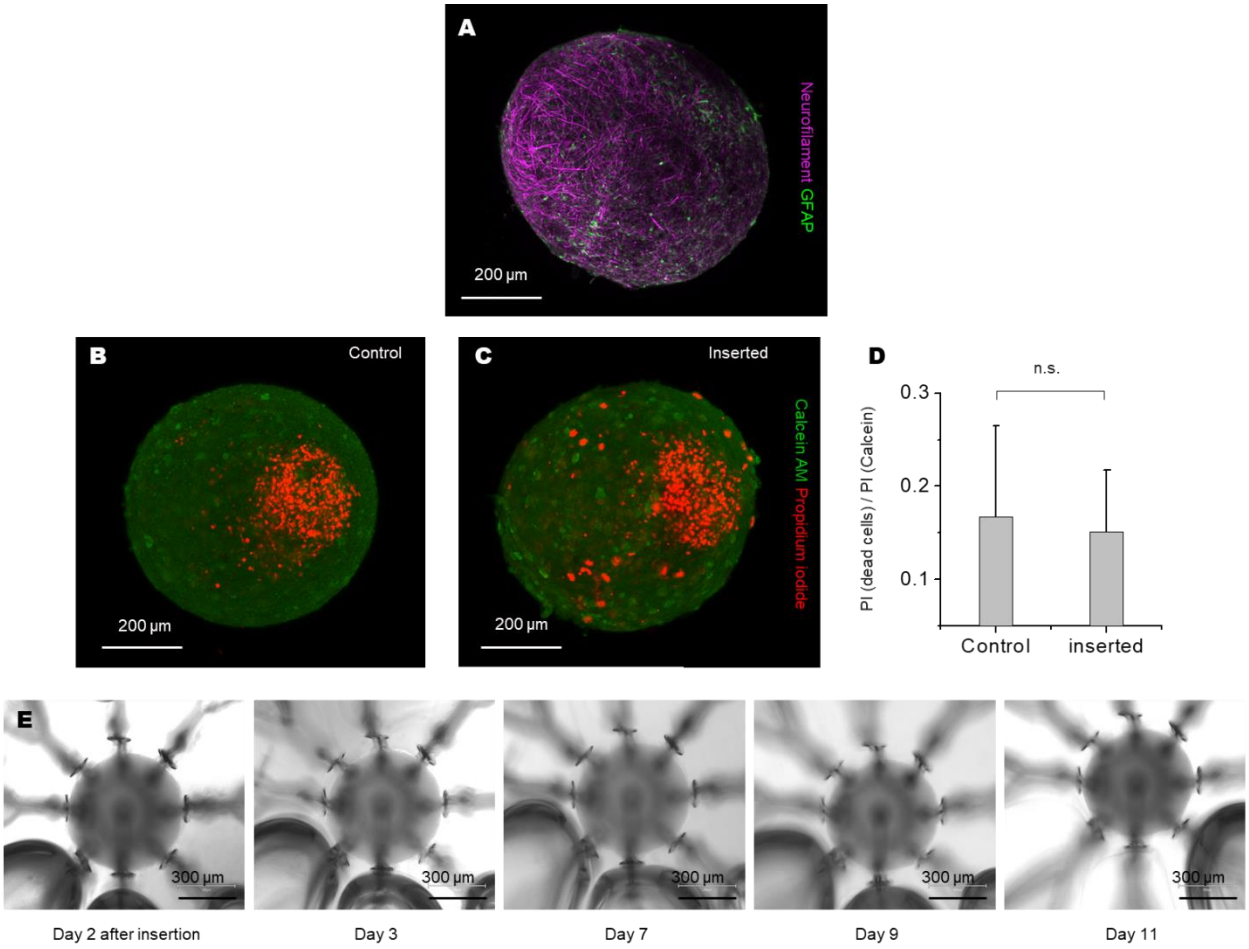

Fig. S9. **Results of confocal microscopy and a cytotoxicity assay.** (**A**) Confocal microscope image of the spheroid; neurofilament (magenta), glial fibrillary acidic protein (green). (**B**) Isolated spheroid (control) and (**C**) spheroid enclosed in a 3D MMF (inserted); Calcein AM (green; live nuclei), Propidium iodide (red; dead nuclei). (**D**) Results that indicate no significant differences (P = 0.7758) between the control and inserted cases; the pixel intensity for red channels is normalized to the intensity of green. (**E**) Optical microscopy images of spheroid after inserting into 3D MMF over 11 d. n=4 control spheroids; n=5 inserted spheroids; two tailed paired T Test; mean ± s.e.m..

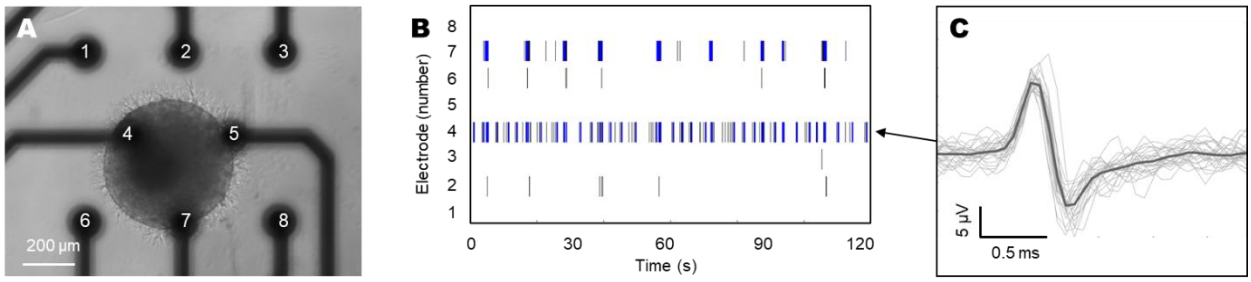

Fig. S10. Spatiotemporal mapping of spontaneous neural activity from a spheroid using 2D MEA. (**A**) Optical images of a spheroid on 2D MEA (Cytoview MEA 6, Axion BioSystems, GA, USA). (**B**) Representative spike raster plots; bursting marked as blue box. **c**, overlay plot of 30 spikes from channels number 4.

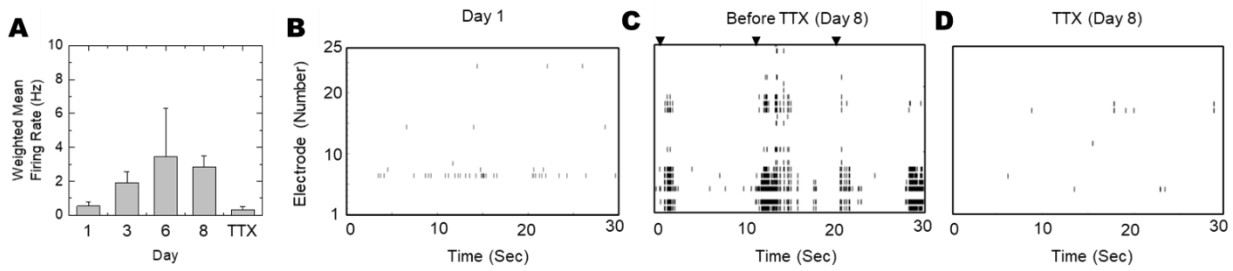

Fig. S11. Weighted mean firing rate and Raster plot over 8 days after insertion. (**A**) Weighted mean firing rate over 8 days after inserting spheroid into 3D MMF**.** (**B-D**) Representative spike raster plots recorded from spheroid at Day 1, 8 before and after applying TTX.

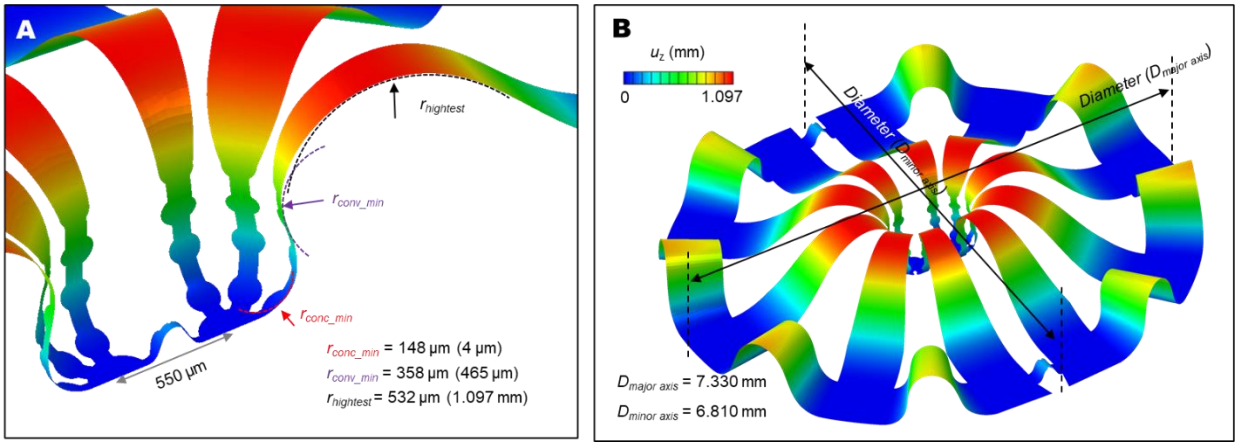

Fig. S12. Key dimensional features of a 3D MMF for assembloid. (**A**) Bending radii over the continuously curved 'wing'. (**B**) Width and height of whole structure of 3D MMF for assembloid.

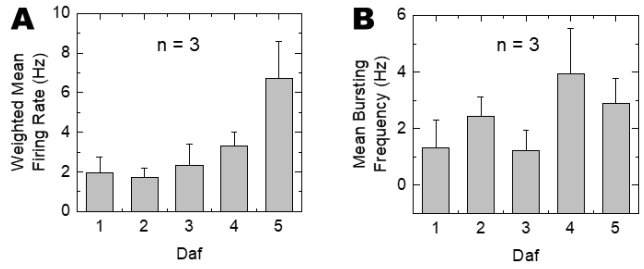

Fig. S13. Weighted mean firing rate and mean bursting frequency over five days after fusion of spheroids. (**A**) Weighted mean firing rate and (**B**) Mean bursting frequency for representative four minutes at each day. n=3 spheroids**.**

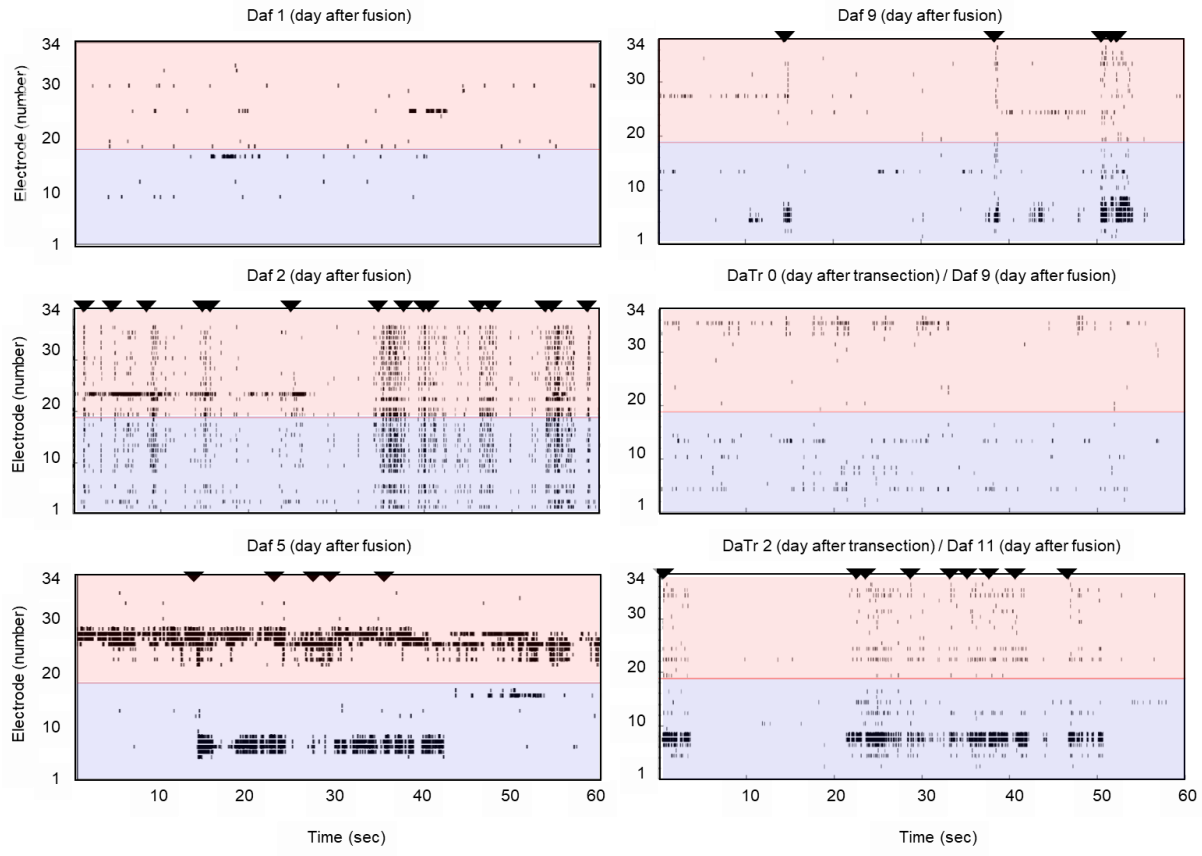

Fig. S14. Representative spike raster plots for network activity of a 3D MMF for assembloid. Representative raster plots recorded from an assembloid that consists of two neural spheroids (red from A, blue from B in Fig. 3) for 60 s over the 1 d to 11 d after fusion (From top left to bottom right).

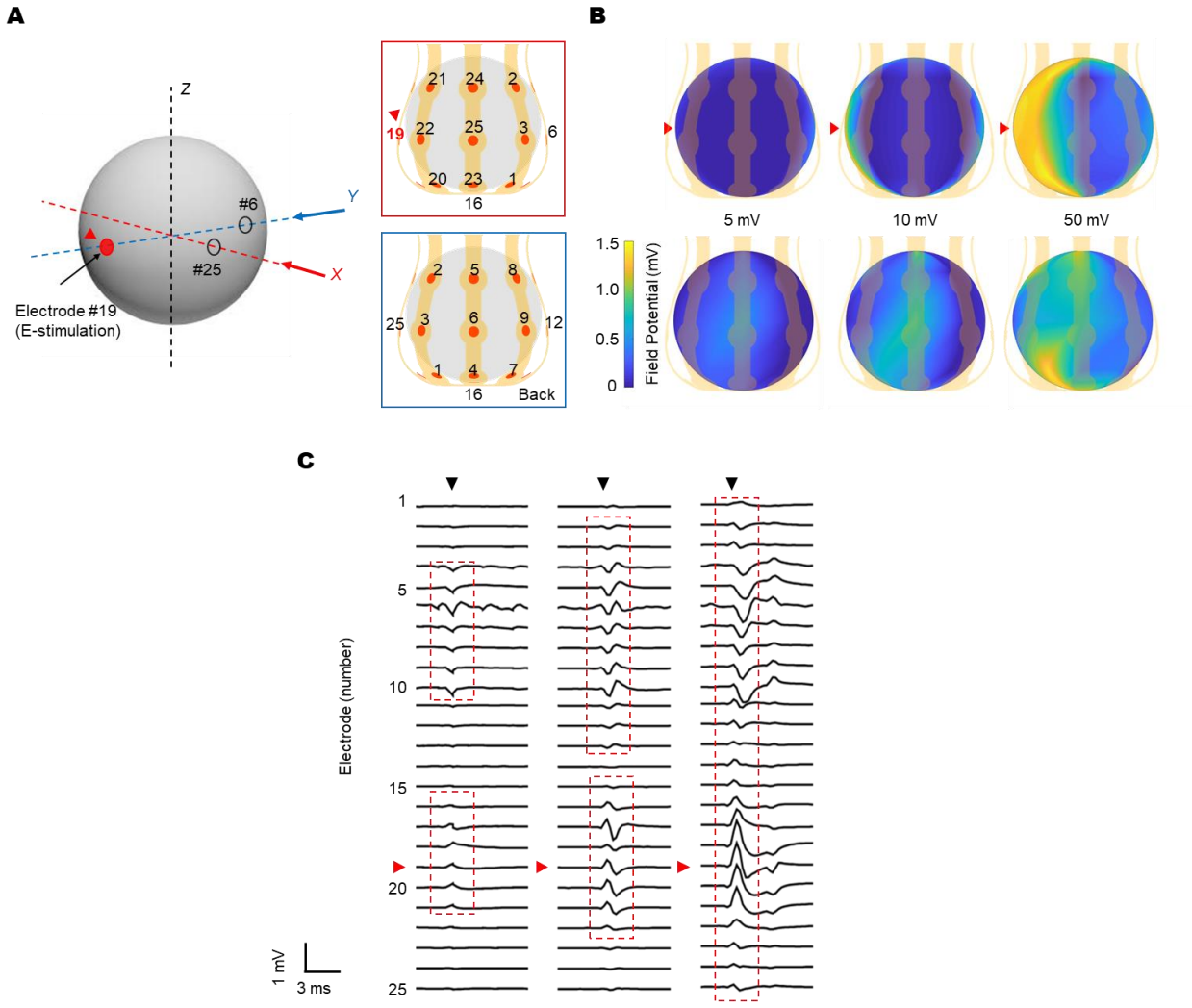

Fig. S15. Electrically evoked responses across a cortical spheroid. (**A**) 3D map of 12 microelectrodes along the X-axis and Y-axis. (**B**) A 3D plot of the amplitude of field potentials along *X*-axis (top) and *Y*-axis (bottom) across the neural spheroid evoked at single electrode (number 19) with a potential of 5 mV (left), 10 mV (middle) and 50 mV (right). (**C**) Representative field potentials from 25 electrodes recorded during electrical stimulation.

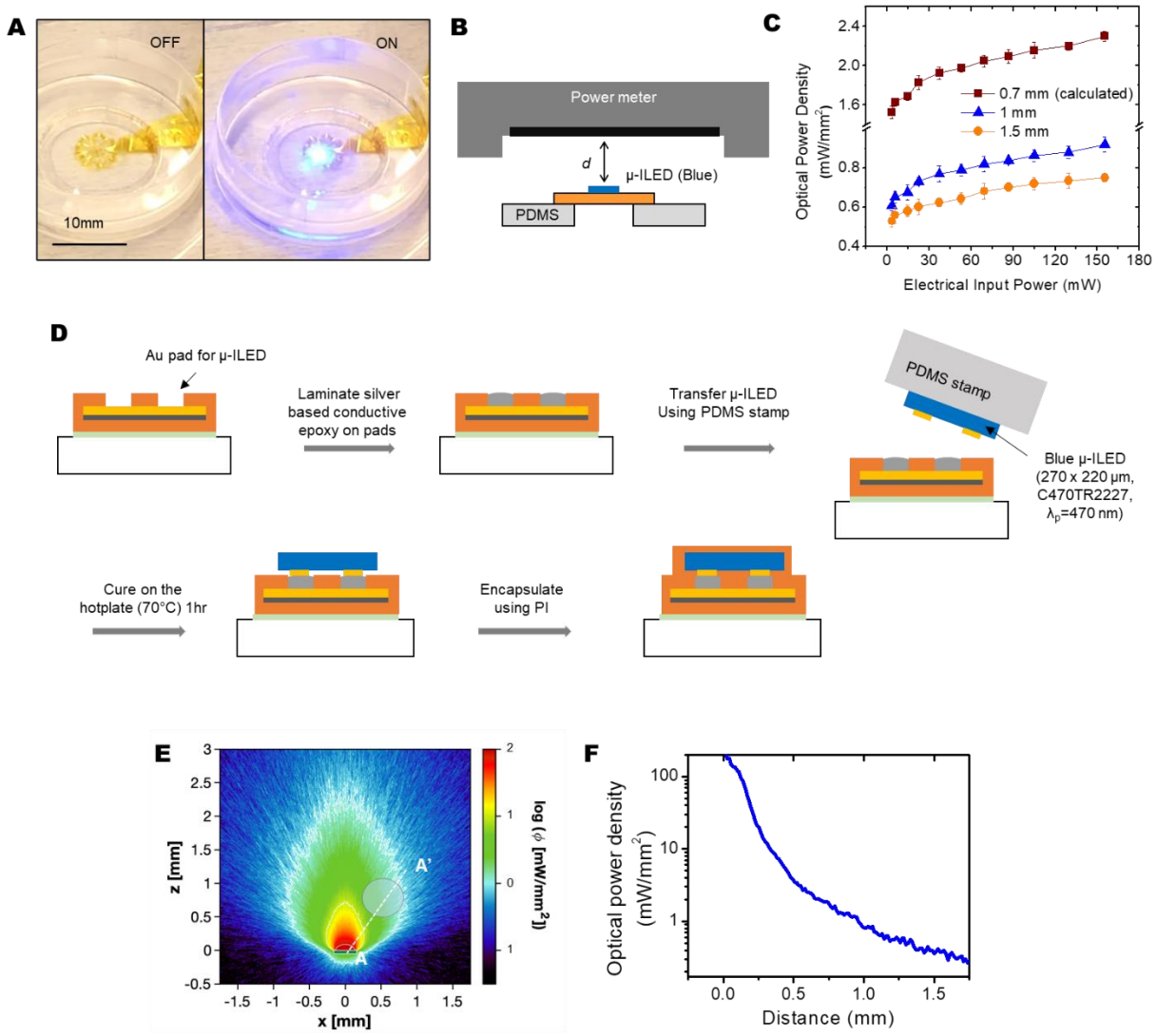

Fig. S16. Schematic illustrations, optical images and modeling results for integration and operation of a μ-ILED in a 3D MMF. (**A**) Picture of a 3D MMF with an integrated blue μ-ILED in the OFF and ON state. (**B**) Schematic illustration of evaluation set-up using a digital power meter (PM100D; power meter and S120VC; photodiode sensor, Thorlab, NJ, USA) placed at different distances (d = 0.7, 1, 1.5 mm) relative to the μ-ILED. (**C**) Measured dependence of the optical power density on the applied electrical power and distance (in air). (**D**) Schematic illustration of steps for integration of an μ-ILED (λ_p = 470 nm, 270 × 220 μm, C470TR2227, Cree, NC, USA) into a 3D MMF. (**E**) Computational results for the optical intensity distribution around the μ-ILED (optical input power = 10 mW) and (**F**) between the μ-LED and the spheroid. Photo credit: Yoonseok Park, Northwestern University.

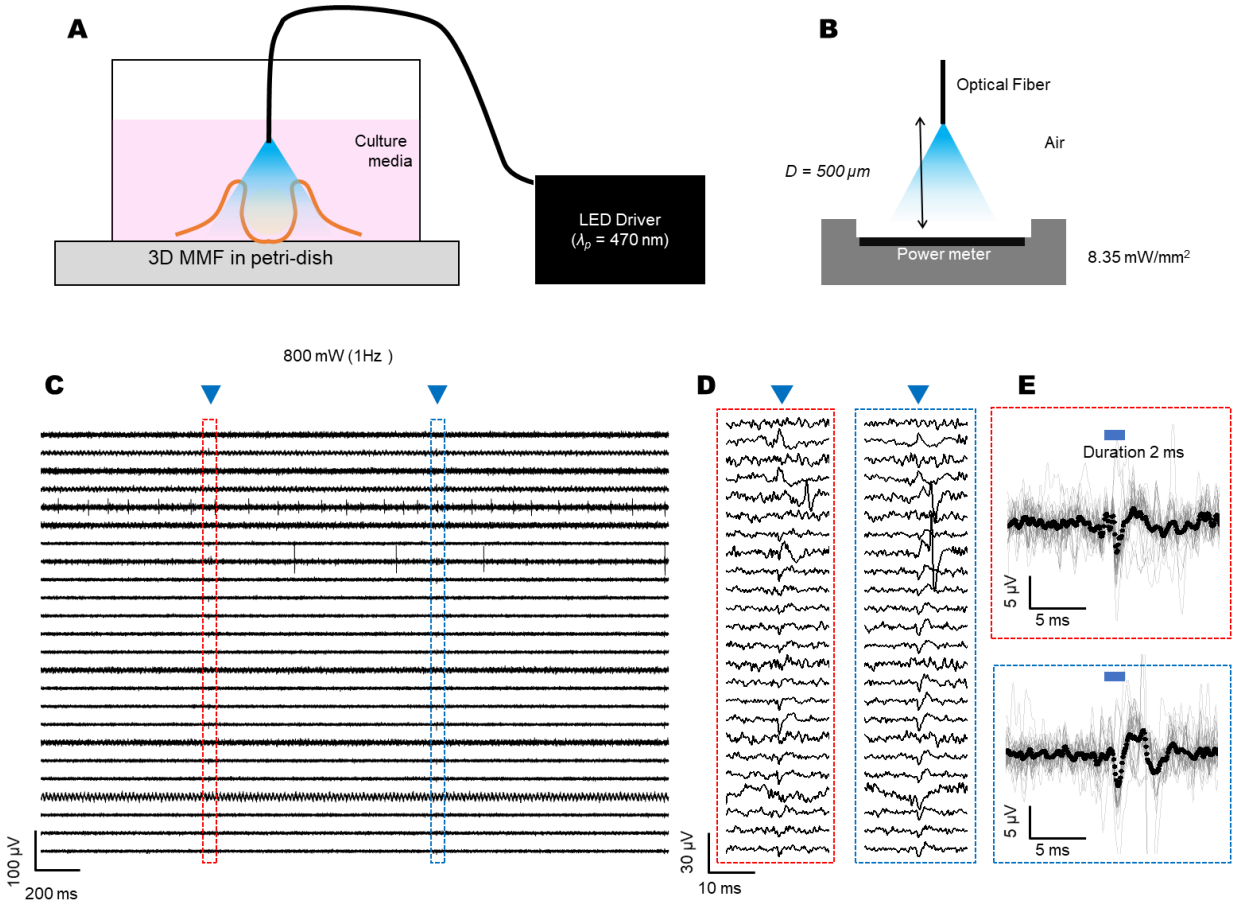

Fig. S17. Optically stimulated responses from a cortical spheroid. (**A**), Schematic illustration of optical stimulation using optical fiber (λ_p = 470nm; fiber-coupled LEDs, M470F3, Thorlab, NJ, USA) and (**B**) optical property evaluation (8.35 mW/mm^2) in air using a digital power meter (PM100D; power meter and S120VC; photodiode sensor, Thorlab, NJ, USA) placed at 500 µm. (**C, D**) representative field potential trace recorded during optical stimulation (P_{input} =800 mW, 1Hz). (**E**) overlaid plots of evoked spikes from 25 channels.

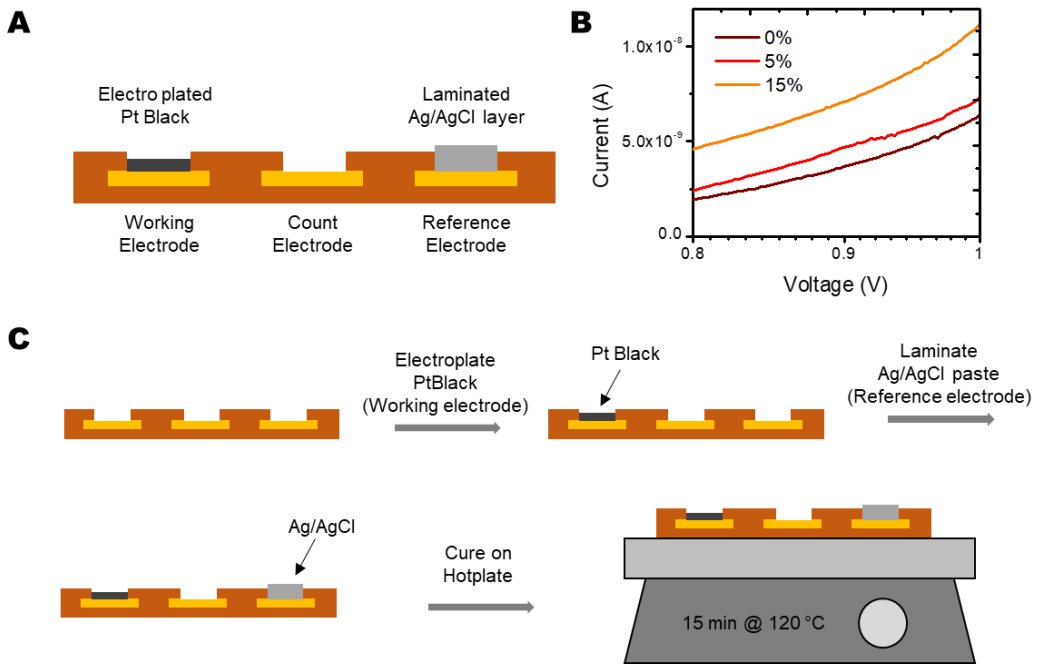

Fig. S18. Design, fabrication and operation of an electrochemical oxygen sensor. (**A**) Schematic illustration of an electrochemical sensor that includes PtBk, bare Au and Ag/AgCl as working, counter and reference electrodes, respectively. (**B**) Cyclic voltammograms for different concentrations of oxygen 0, 5, 15%. (**C**) Schematic illustration of steps for integration of an electrochemical sensor into a 3D MMF.

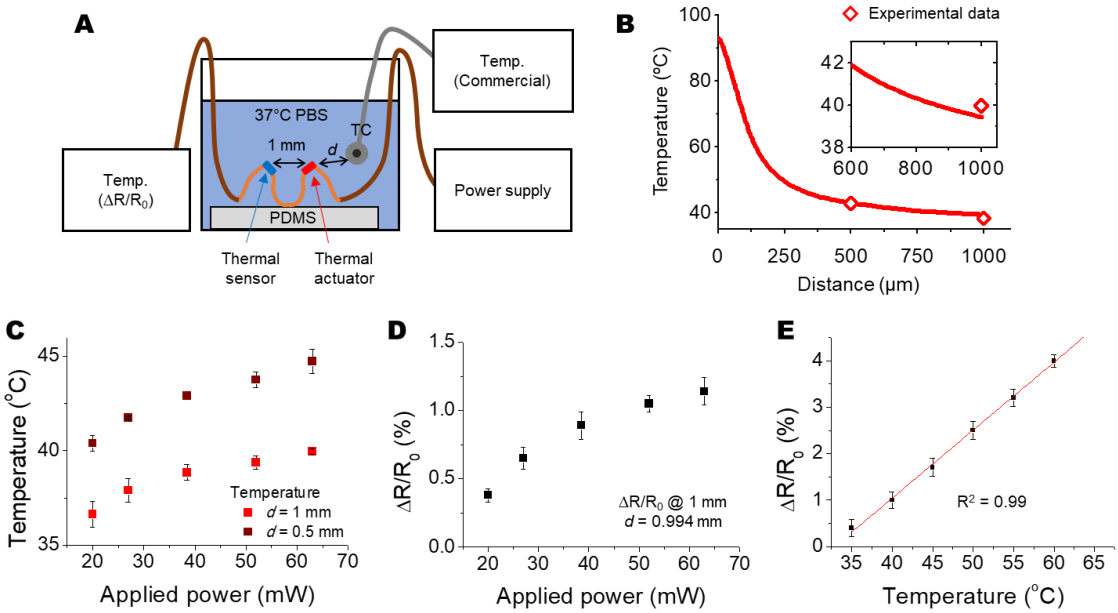

Fig. S 19. Schematic illustration of characterization setups and measurement results for operation of the thermal actuator. (**A**) Schematic illustration of the thermal actuator and temperature sensor immersed in PBS along with a commercial thermocouple. (**B**) Computed distribution of temperature between the thermal actuator ($P_{applied}$ = 38mW) and the spheroid (d = from 600 μm to 1 mm) and the temperature sensor (~1 mm), together with experimental data. (**C**) Temperature measured using the thermocouple in PBS at d = 500 μm and 1 mm as a function of applied power. Measured change in resistance of the thermal sensor as a function of (**D**) applied power and (**E**) temperature of PBS controlled by a hotplate.

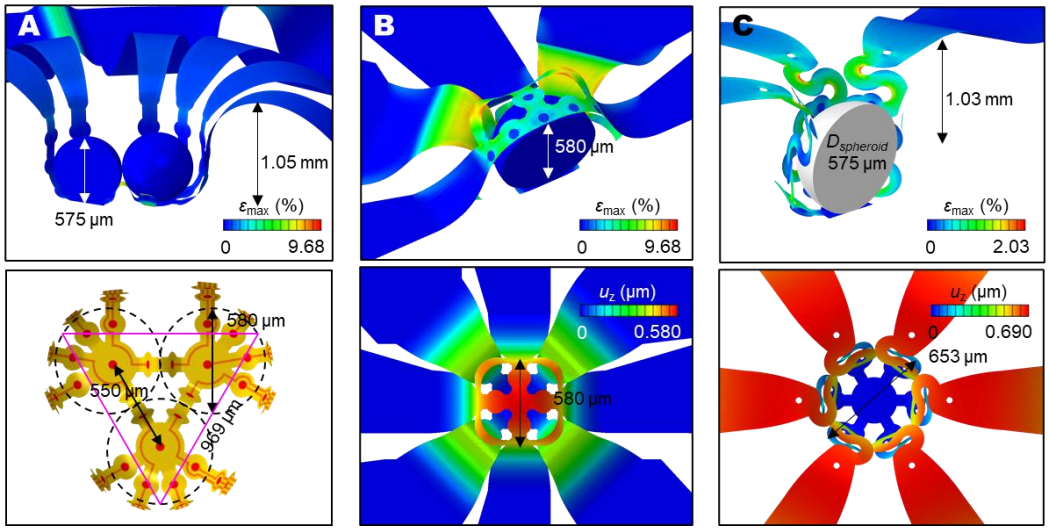

Fig. S20. Dimensional information for a set of complex 3D MMFs by FEA. Maximum height and lateral dimensions information of the 3D MMF (**A**) with a layout that accommodates three organoids, (**B**) with a full coverage across the an entire 4π solid angle and (**C**) with deformable, serpentine structural elements.

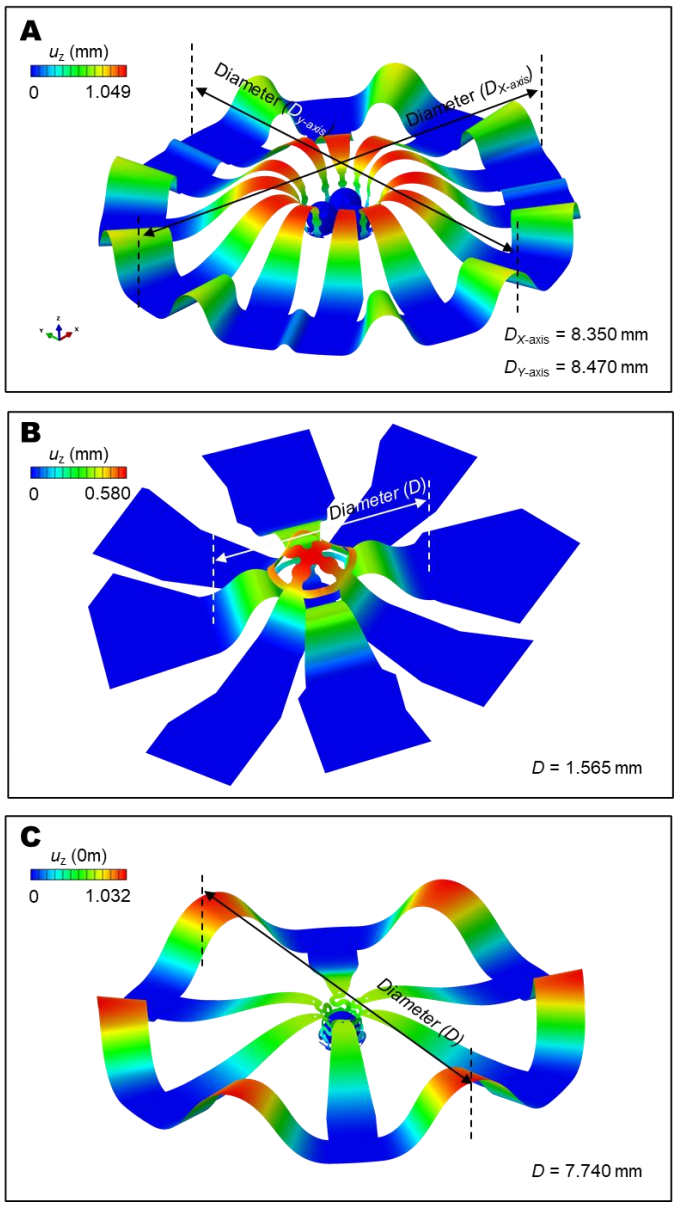

Fig. S21. Key dimensional aspects of advanced 3D MMFs. Lateral dimensions information of the whole 3D MMF (**A**) with a layout that accommodates three organoids, (**B**) with a full coverage across the an entire 4π solid angle and (**C**) with deformable, serpentine structural elements.

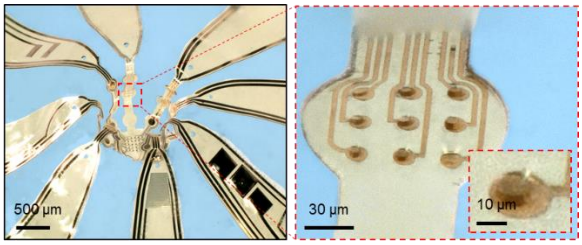

Fig. S22. Optical micrographs of a 3D MMF with a high-density array of microelectrodes. Optical image of a high-density array of electrodes on a 3D MMF (9 electrodes in an area of 60 × 60 µm; electrode size 10 µm; distance between electrodes 30 µm). Photo credit: Yoonseok Park, Northwestern University.

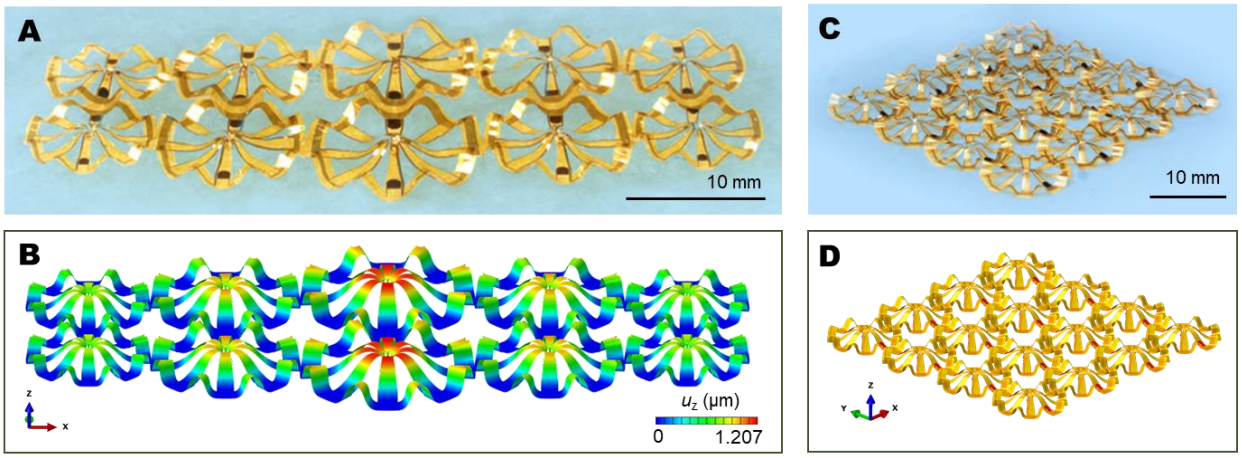

Fig. S23. 3D MMF arrays. Optical micrograph and FEA modeling of 3D MMF arrays. Photo credit: Yoonseok Park, Northwestern University.

Supplementary Note 1.

Pre-plated, ready to use, 3D neurospheroids composed of cortical neurons and astroctyes were obtained from StemoniX, Inc. (microBrain 3D®, StemoniX Cat # BSARX-AA-0384). Neural spheroids were generated from human induced pluripotent stem cells (hiPSCs) as described previously(*19*,*20*). Briefly, neural progenitor cells (NPCs) were isolated from hiPSCs-derived neural rosettes(*19*), cultured in spheroid format, and matured into cortical neurons and astrocytes(*20*). RNA-Seq analysis demonstrates cortical identity through expression of cortical layer genes (RELN, NDNF, CNR1, POU3F3, and BCL11, see Fig. S7) while synchronized spontaneous activity along with astrocyte, neuronal, and synaptic markers demonstrate the presence of functional neural structure. These spheroids contain astrocytes and neurons at a ratio of about 1:1. The neurons express MAP2, indicating that they are mature, and synapsin I, indicating the presence of synapses. This data is consistent with the robust, spontaneous, synchronous, electrophysiological activity of these cultures, which demonstrates functional maturity and connectivity. Neurotransmitter receptor and ion channel genes are expressed in these spheroids at levels similar to their expression in human brain(*21*).

Upon receipt from the Manufacturer, the medium was changed (1/2 volume, 3 times) using BrainPhys Neuronal Medium SM1 Kit (StemCell Technologies, No. 05792, BC, Canada) supplemented with 20 ng/ml of recombinant human BDNF (StemCell Technologies, No. 78005, BC, Canada), 20 ng/ml of GDNF (StemCell Technologies, No. 78058, BC, Canada), and 1X Penicillin-Streptomycin (GE Healthcare Life Sciences, PA, USA) or the NeuralX Cortical Neuron media kit that follows a recipe published by Bardy et al.(*44*) (StemoniX, NXCNM-AA-0250, MN, USA). Spheroids were maintained at 37 °C and 5% CO2 until used in experiments. Half media changes were performed every Monday, Wednesday, Friday using one of the two above described media. Manufacturing batch consistency and media equivalency was confirmed as spheroid activity and size were highly reproducible across manufacturing lots and culture media (see Supplementary Table 1).

Supplementary Note 2.

Polyimide and parylene-C have comparable elastic modulus and Poisson's ratio of E_{PI} = 2.5 GPa, ν_{PI} = 0.34 and $E_{parylene}$ = 2.76 GPa, $\nu_{parylene}$ = 0.4, respectively, making the 3D devices made of either polyimide or parylene-C mechanically similar. Moreover, when the elastic substrate is sufficiently stiff (sufficient combination of thickness and elastic modulus), the 3D device is controlled and the final 3D geometry is independent of material elastic modulus of the 3D device; In our design, the elastomer substrate made of PDMS can be assumed sufficiently stiff compared with Polyimide and parylene-C.

Supplementary Note 3.

Tests of optical stimulation without the spheroid yield no measurable responses. Operation of the integrated μ-ILED requires electrical isolation to avoid the introduction of noise in the metal traces for the electrodes. The optical fiber eliminates this source of noise**.**

Supplementary Table 1 Spheroid reproducibility across manufacturing batches and culture media. Manufacturing batch represents independent production runs that were cultured in either NeuralX or BrainPhys culture media. Activity is measured as the number peaks shown by the synchronized, spontaneous, oscillatory spheroid activity measured as Ca2+ waveforms as previously described[23] and expressed as the mean across at least XYZ test wells in each plate. Size was measured as spheroid diameter captured with XYZ microscope for all spheroids in the test 384 well plates from each manufacturing batch.

	Average Activity (peaks / 10 min.)		Average Spheroid Diameter (µm)	
Manufacturing Batch	NeuralX	BrainPhys	NeuralX	BrainPhys
A	8.3	4.1	649	681
B	5.6	4.2	653	697
C	5.2	9.3	625	691
D	6.8	4.3	695	586
E	4.6	6.6	662	676
Mean +/- SEM	6.1 ± 1.3	5.7 ± 2.0	656.8 ± 11.3	666.2 ± 20.4

Supplementary table 2. Age and lot number of spheroids from Stemonix

		Age of Spheroid (Day 0, DaF 0)	lot number from StemoniX
Spheroid	1	10w	20190707-01
	2	12w	20190707-01
	3	14w	20190707-01
Assembloid	1	14w	20190417-01
	2	10w	20190707-01
	3	13w	20190707-01